nature communications

Article

https://doi.org/10.1038/s41467-025-56502-9

Bioinspired interfacial engineering for highly stretchable electronics

Received: 19 June 2024

Accepted: 17 January 2025

Published online: 04 February 2025

Check for updates

Osman Gul[1,2], Myoung Song[1], Chang-Yeon Gu[1], Jihyeon Ahn[1], Kichul Lee[1], Junseong Ahn[3], Hye Jin Kim[2,4] ✉, Taek-Soo Kim[1] ✉ & Inkyu Park[1] ✉

The seamless integration of rigid/flexible electronic components into stretchable substrates is imperative for the realization of reliable stretchable electronics. However, the transition from flexible-to-stretchable substrates presents inherent challenges in interfacial behavior, predominantly arising from disparities in elastic moduli, thereby rendering their integration arduous for practical deployment. Here, we introduce a bioinspired interface-engineered flexible island (BIEFI), which effectively facilitates the creation of highly stretchable electronics by optimizing the interface with flexible mechanical interlocking mechanisms, resilient to physical deformations. Various electronic components, such as light-emitting diodes (LEDs) and solar cells, are affixed onto the flexible island, showcasing its versatility as a robust platform for rigid components while ensuring the entire substrate maintains high stretchability. Additionally, a smart workout monitoring system is demonstrated by integrating a resistance band with a flexible-to-stretchable platform. This approach seamlessly integrates a wide range of rigid, flexible, and stretchable components, ensuring durability under diverse physical deformations.

Flexible and stretchable electronics have been a core focus of emerging research fields, which show high potential for shaping the future electronics world[1–4]. Flexible electronics, which enable circuits and electronic components, show their functionality under limited physical deformations such as bending[5,6]. Stretchable electronics enable safe operation under diverse physical deformation modes such as stretching, twisting, and so on[7]. The potential of stretchable electronics opens a new road for electronics, such as wearable devices[8–10], displays[11,12], and energy harvesters[13–15].

Although numerous progresses have been made in developing stretchable electronics, integrating rigid, flexible substrates into the stretchable substrate remains challenge. The mismatch in mechanical properties, particularly the difference in elastic moduli between rigid and stretchable substrates, often leads to performance failures when subjected to stretching. Addressing this issue requires innovative designs that can effectively isolate and distribute strain, minimizing the concentration of mechanical stress at the interface between rigid and stretchable materials. There have been several efforts with different approaches to enhance stretchability by modifying the geometry (e.g., serpentine, kirigami, and rigid island)[16,17]. The serpentine and kirigami approaches have used flexible substrates such as polyimide (PI) and polyethylene terephthalate (PET) to build stretchable electronics[18,19]. In these examples, the flexible substrate is strategically designed and fabricated to achieve stretchability. However, these solutions are limited in their ability to fully mitigate the strain mismatch at the rigid-stretchable interface, leading to failure over extended use. On the other hand, the rigid island approach is used to minimize the mismatch of the elastic modulus of the rigid island and stretchable substrate with several strategies, such as material-based and interfacial engineering-based methods. Material-based

[1]Department of Mechanical Engineering, Korea Advanced Institute of Science and Technology (KAIST), Yuseong-gu, Daejeon, Republic of Korea. [2]Intelligent Components and Sensors Research Section, Electronics and Telecommunication Research Institute (ETRI), Yuseong-gu, Daejeon, Republic of Korea. [3]Department of Control and Instrumentation Engineering, Korea University, Sejong, Republic of Korea. [4]Department of Advanced Device Technology, University of Science and Technology, Daejeon, Republic of Korea. ✉e-mail: nolawara@etri.re.kr; tskim1@kaist.ac.kr; inkyu@kaist.ac.kr

approaches use material's stiffness gradients to lower the discrepancy between high and low elastic moduli to increase the stretchability of the device[20–23]. The challenges in previous studies include issues with scalability, as complex multi-step fabrication processes limit practicality for large-scale applications. Additionally, maintaining long-term durability and stability under repeated strain has been a significant obstacle, leading to performance degradation over time in some designs. Mechanical mismatches between rigid and soft materials, as well as difficulties in embedding rigid components into flexible substrates, further hinder overall flexibility and application potential in many approaches. A recent study of an interfacial engineering-based approach utilized the mechanical interlocking method[24]. However, the proposed rigid island made from polyactic acid (PLA) demonstrated low flexibility and significant thickness, restricting its use in various flexible and stretchable electronics applications (Supplementary Table 1).

In nature, plant roots anchor themselves deeply into the soil to enhance the interface (roots-soil interlocking), thereby reducing the mismatch between the rigid plant body and the soft soil structure[25]. Moreover, the root structure contributes to standing firmly on the ground and enduring harsh conditions: weather and natural disasters. Roots-soil interlocking postulates high adhesion and secure interfacial behaviors and is also shown in mimicking applications such as stretchable electrodes[26] and structural batteries[27].

Herein, we develop bioinspired interfacial engineered flexible islands (BIEFI) demonstrating high stretchability and establishing excellent physical deformational performances for flexible-to-stretchable electronics (Fig. 1a). Inspired by roots-soil structure, the flexible-to-stretchable interface is designed using a flexible substrate with root structures embedded within a stretchable substrate (Fig. 1b). By conducting a parametric study in the BIEFI design, optimized to facilitate a flexible interlocking mechanism, significant improvement in stretchability up to 700% strain can be achieved. (Fig. 1c). The flexible mechanical interlocking mechanism extends the fatigue life for various types of physical deformations (e.g., strain, poking, and twisting). The optimized BIEFI design demonstrates applications of flexible-to-stretchable platform (e.g., stretchable LED array and solar cell array) under diverse physical deformations (Fig. 1d). A smart resistance band (SRB) was developed to show highly stretchable applications by integrating the optimized BIEFI into a resistance band that monitors workout with a strain sensor and accelerometer (Fig. 1e). The proposed strategy facilitates a new perspective on the integration of rigid, flexible, and stretchable components with optimized BIEFI design for high stretchability and endurance for flexible-to-stretchable platform. It also paves the way for exploring the commercial feasibility of stretchable electronics.

Results

Design and mechanism of Bioinspired Interfacial-Engineered Flexible Island

The interfacial interlocking mechanism of roots-soil in trees are utilized to create a flexible-to-stretchable structure for stretchable electronics in this work (Fig. 2a). To build a flexible-to-stretchable platform, specifically BIEFI design, the materials for flexible island and stretchable substrate were chosen as Polyimide (PI) (modulus: 3.2 GPa)[6], and Ecoflex (modulus: 50 kPa)[28], respectively. Root structure possesses primary and secondary roots, enhancing its effective and secure ground gripping through these diverse root types (Supplementary Fig. 1).

Figure 2b demonstrates the parameters of the proposed roots-soil model for BIEFI. When the dimensions of flexible island width (a = 20 mm), primary root length (b = 10 mm), and secondary root length (Ra = 1 mm) are fixed, the width of the roots (K) were selected as 70, 100, 200, and 300 µm. The width range of each primary and secondary root can be calculated for equal spacing using Eqs. (1) and (2), respectively.

$$w = \frac{a - N \times K}{K + 1} \tag{1}$$

$$Rw = \frac{b - Rn \times K}{K + 1} \tag{2}$$

where N, w, and Rw are the number of roots, the gap between primary roots, and the gap between secondary roots, respectively. Thus, the values of N and Rn ranged from 0 to 12 due to design limitations. Adjusting the parameters creates 13 different design cases for the rootless to primary root structure (Supplementary Table 2). On the other hand, including secondary root parameters in the primary root structure builds 48 different design cases (Supplementary Table 3).

The BIEFI is fabricated by the UV laser-cutting of PI and then embedded into Ecoflex. The detailed fabrication process is demonstrated in Supplementary Fig. 2 and explained in the experimental section. Interfacial failure under strain in the PI embedded within the Ecoflex structure can be observed visually. However, to accurately investigate the transition zone effect of the flexible-to-stretchable interface, a quantitative measurement method is required. Therefore, the Ecoflex on PI was removed to conduct tensile tests (Fig. 2c and Supplementary Fig. 3). The uniaxial tensile test setup is shown in Fig. 2d. Through this setup, quantitative tensile test data was acquired to identify the interfacial failure with load drop successfully.

The BIEFI shows high stretchability with the proposed primary and secondary roots. The primary roots act as a stress distribution structure to delay the interfacial failure. The secondary roots serve as a mechanical interlocking structure to suppress the interfacial failure. It is revealed that the optimized secondary roots securely grasp the elastomer and exhibit flexible movement under strain, a phenomenon referred to as the flexible interlocking effect. In the optimized structure of BIEFI, as shown in Fig. 2e, with the application of strain, each secondary root gets affected by the strain and moves in the direction of the strain with the flexible interlocking effect. After the secondary root reaches its maximum allowable flexible deformation, the adhesive effects contribute until it reaches its maximum adhesion fracture point. This process is repeated until the entire root structure is affected by strain, leading to the interfacial failure. The images of the sample under 0% and 400% strains are shown in Fig. 2f. It can be observed that secondary roots exhibit flexible movements under applied strain.

Parameter study and optimization of the BIEFI

To optimize the BIEFI design, the effects of three different dimensional parameters such as number of primary roots (N), number of secondary roots (Rn), and width of the roots (K) were examined. A specific design code is assigned for each BIEFI design case to denote its dimensional parameters (Supplementary Tables 2 and 3). The design code follows the format of (parameter abbreviation)(value). For example, $K100N3$-$Rn3$ denotes that the width of a root is 100 µm, the primary root number is 3, and the secondary root number is also 3. The parameter study can be approached in two ways: first by optimizing N, followed by Rn and K, or by optimizing N, followed by K, and then Rn (Supplementary Fig 4). Initially, to process the parameter study on the effect of the number of primary roots (N), the width of the roots was fixed at 100 µm. Strain tests were conducted for K0N0 (Rootless Island (RLI)) to K100N12 design (Fig. 3a). The introduction of primary roots into the design has shown an increase in the strain at failure value. An increase in the number of primary roots also leads to a higher strain at failure value, attributed to the stress distribution effect caused by the primary roots under strain. The K100N12 design shows a 270% increase in the stretchability compared to RLI; the parameter study on the effect of a number of secondary roots (Rn) proceeded with the K100N12 design (Fig. 3b, c). While the number of secondary roots increases, strain at

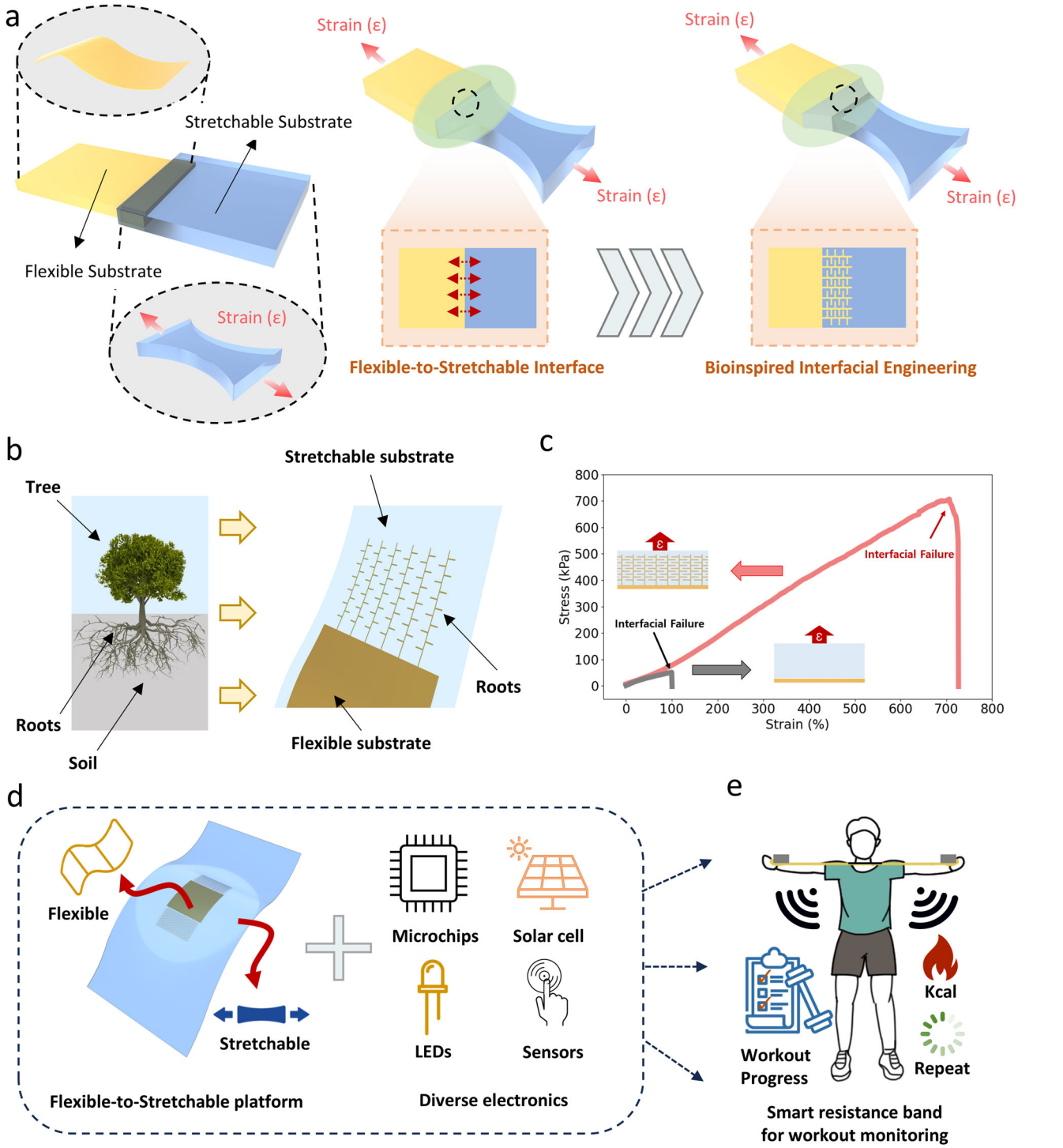


Fig. 1 | Bioinspired Interface-Engineered Flexible Island (BIEFI) within stretchable substrate for highly stretchable flexible-to-stretchable platforms. **a** Schematic illustration of flexible-to-stretchable substrate interface with bioinspired interfacial engineering. **b** Roots-soil inspired flexible-to-stretchable interface design. **c** Stress versus strain comparison for the Rootless Island (RLI) (gray line) and BIEFI (red line) embedded in Ecoflex under stretching. **d** Schematic of BIEFI applications in the flexible-to-stretchable platform for stretchable electronics applications with diverse electronic devices. **e** Schematic of application of BIEFI for highly stretchable electronics: Smart resistance band for workout monitoring. Source data are provided as a Source Data file.

failure increases correspondingly. The K100N12-Rn12 design exhibits an 89.2% increase compared to the K100N12 design (Fig. 3d). Due to the flexible mechanical interlocking effect of secondary roots, the stretchability of BIEFI was significantly improved. The minimum width value of the roots (*K*) was set as 70 μm due to the limited resolution of UV laser cutting. Also, 300 μm was set as the maximum value for the width of the roots (*K*) because of design limitations (Fig. 3e). K100N12-Rn12 has shown a 20.7% increase compared to the K70N12-Rn12 design (Fig. 3f). On the other hand, if the width of the roots (*K*) increased larger than 100 μm, a significant decrease in the strain at failure has been observed. As the root structure functions as an anchoring mechanism within the elastomer, its strength is crucial. When the root width is less than 100 μm, it cannot firmly grasp the elastomer, leading to easy deformation and rapid failure under applied strain. If the root

https://doi.org/10.1038/s41467-025-56502-9

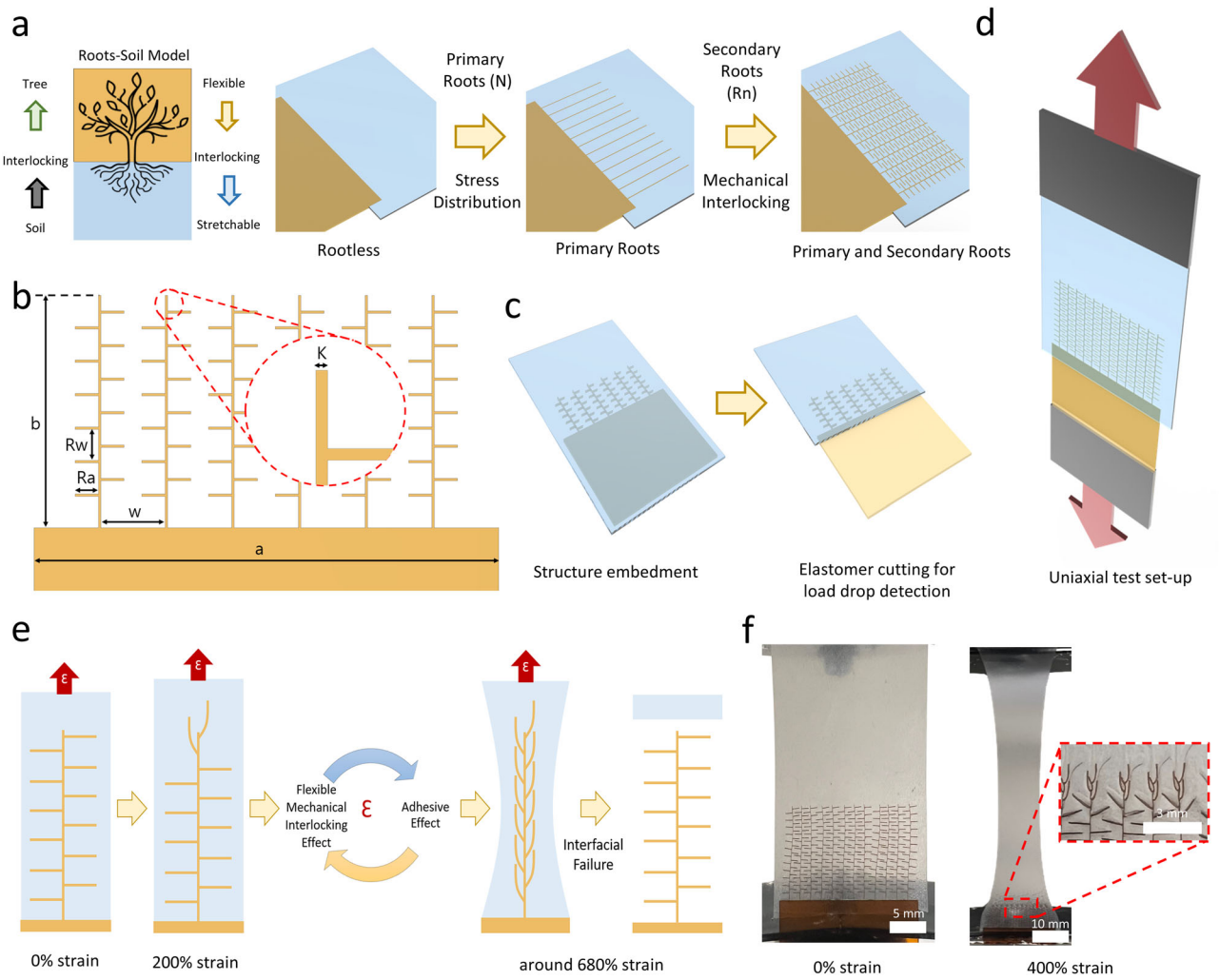


Fig. 2 | BIEFI design, parameter study, and working mechanism. a Schematic illustration of the procedure for obtaining BIEFI. **b** Parameters of BIEFI design: flexible island width: a, root width: K, primary root length: b, gap between primary roots: w, secondary root length: Ra, and gap between secondary roots: Rw. **c** BIEFI and stretchable substrate design for load drop detection during interfacial failure. **d** Schematic of strain experiment test set-up for BIEFI. Black color: clamping area. **e** Schematic illustration of BIEFI working mechanism with flexible mechanical interlocking and adhesive effects. **f** Photograph of optimized BIEFI under strain applications; left: 0% strain, right: 400% strain.

width exceeds 100 µm, its strength greatly increases, limiting its flexibility under applied strain. Consequently, this rigidity leads to fractures in the elastomer. Therefore, the parameter study confirmed that the K100N12-Rn12 design shows the optimal result with a 600% increase in the stretchability compared to the RLI design. Furthermore, performing the parameter study in both approaches as Supplementary Fig. 4 yields the same optimal design, which is K100N12-Rn12.

The stretchability of the structure is significantly influenced by the modulus of the stretchable substrate. To investigate this, we conducted comparative experiments between Dragon Skin, which has a modulus approximately twice that of Ecoflex, and Ecoflex itself. The results indicated that the RLI design in Dragon Skin experienced interfacial failure at 65% strain, whereas the K100N12-Rn12 design in Dragon Skin endured strains up to around 300% (Supplementary Fig. 5). These findings suggest that the bioinspired root structure significantly enhances the stretchability of flexible-to-stretchable interfaces. The experimental results and comparative analysis demonstrate that the mechanical properties of the stretchable substrate play a critical role in determining both stretchability and interfacial stability in flexible-to-stretchable interfaces. Ecoflex allows for higher stretchability (up to 700% strain) and better interfacial adhesion, as it conforms more effectively to the root structure. In contrast, Dragon Skin exhibits reduced stretchability (up to 300% strain) and is more prone to interfacial failure. The increased stiffness of Dragon Skin leads to greater stress concentrations at the interface between the rigid and stretchable components, limiting its ability to accommodate large deformations. In the initial design of flexible-to-stretchable interface, the root length (*b*) is fixed at 10 mm to thoroughly investigate various parameters. Additionally, the effect of different root lengths was explored to understand better its effect on the strain at failure. The minimum root length was fixed at 2 mm and incrementally increased by 2 mm to evaluate its effect on the optimal design for strain at failure (Supplementary Fig. 6). The experimental results demonstrated that a 2 mm interface length could achieve 400% stretchability. Moreover, the experimental results showed that interface lengths of 4 mm, 6 mm, and 8 mm could achieve stretchability of 460%, 510%, and 600, respectively.

To investigate the omnidirectional behavior of the optimized BIEFI design, we designed omnidirectional BIEFI as shown in Fig. 3g–h. The uniaxial test results exhibit that omnidirectional root design shows strain at failure value at 400% around 360°, while a circle (without root design) shows strain at failure result in around 100% (Fig. 3i). Furthermore, to investigate the effect of the angle of the secondary roots, the secondary roots designed as 30° declined against the strain direction. It is observed that 30-degree declined secondary roots show a 10% increase in strain at failure (Supplementary Fig. 7). The serpentine

https://doi.org/10.1038/s41467-025-56502-9

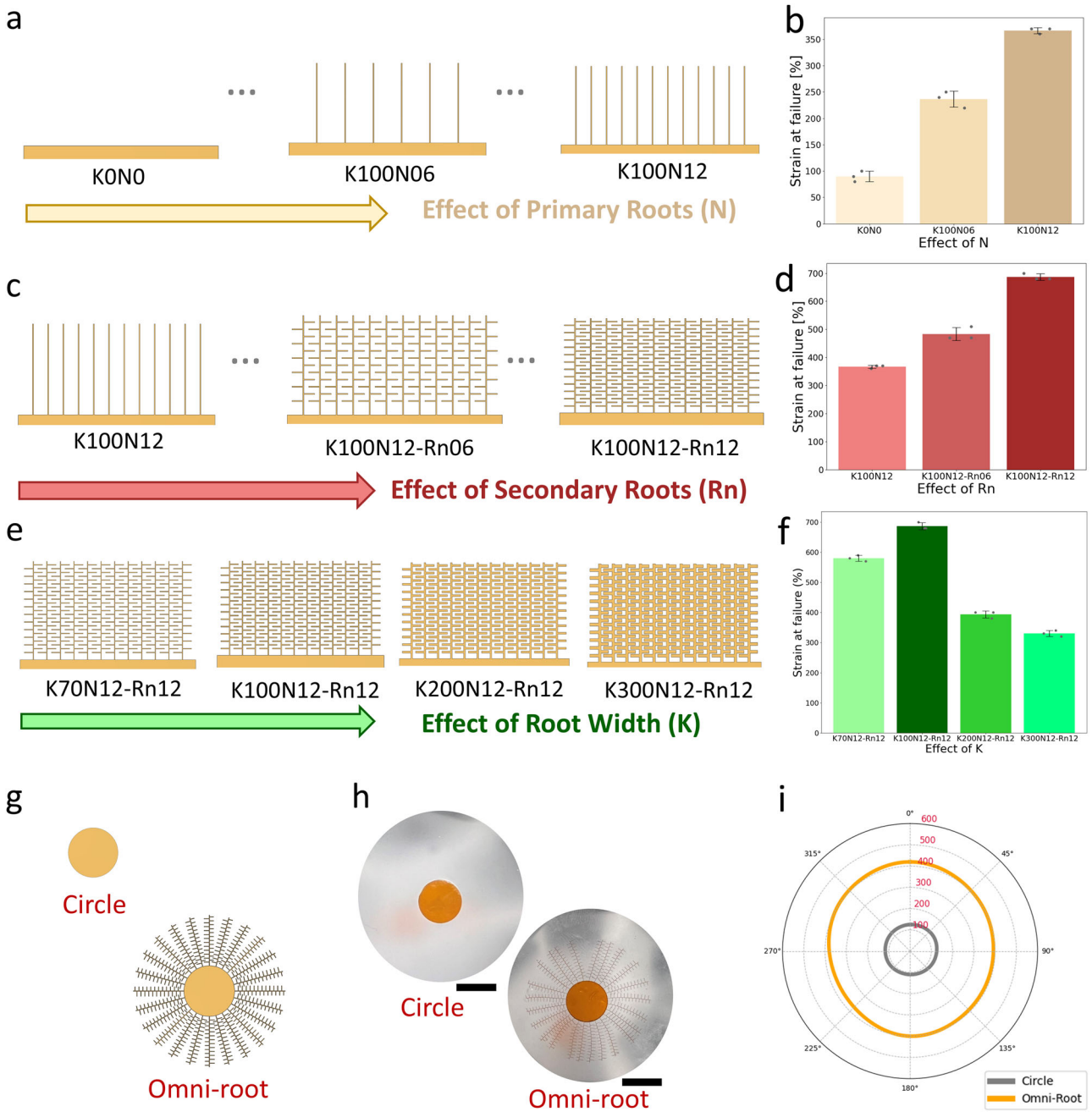


Fig. 3 | Parameter optimization process of BIEFI. a Design of primary roots with varying root numbers. **b** Experimental results of the effect of primary roots in the strain at failure. **c** Design of secondary roots with varying root numbers. **d** Experimental results of the effect of secondary roots in the strain at failure. **e** Design of roots with varying root widths. **f** Experimental results of the effect of root width in the strain at failure. Data are presented as mean values ± SD, where $n = 3$ technical replicates. **g** Schematic illustration of the RLI circle and the omni-directional design of BIEFI. **h** Photographs of the omnidirectional RLI and BIEFI. Scale bar 10 mm. **i** The strain at the failure diagram depends on the angle. Omni-directional designs rotated at specific angles were applied to uniaxial tensile stretching to detect strain at failure. Source data are provided as a Source Data file.

pattern offers limited stretchability to flexible substrates. To better understand the effect of more diverse structures at the flexible-to-stretchable interface, we designed the primary roots in a serpentine pattern and investigated its effect on strain at failure (Supplementary Fig. 8). The integration of the serpentine pattern into the primary roots increased the strain at failure of the K100N12-Rn12 design by 10% as shown in Supplementary Fig. 9. Moreover, the impact of the thickness of the optimized BIEFI has been investigated with thicknesses of 100, 50, and 25 μm of PI (Supplementary Fig. 10). A decrease in the thickness of the island leads to a reduction in the strain at failure. This can be explained by acknowledging that thickness is also a crucial parameter influencing the fundamental strength of BIEFI. As previously mentioned above, if the root width decreases below 100 μm, lower strain at failure value is observed (Fig. 3f). Similarly, if the root thickness decreases below 100 μm, it also results in a lower strain at failure value. These two parameters, root width and thickness, highly affect the root's ability to firmly grasp the elastomer.

Finite element analysis simulation and mechanical behavior of the BIEFI

To clarify the mechanism of the highly stretchable BIEFI, a finite element analysis (FEA) was conducted. Representative models for the

https://doi.org/10.1038/s41467-025-56502-9

rootless interface, interface with a primary root, and that with additional secondary roots were prepared as shown in Fig. 4a. While the end of flexible PI was fixed, the end of stretchable Ecoflex was stretched in *y*-direction with displacement-controlled loading, the interface between PI and Ecoflex was defined by the fracture criterion based on virtual crack closure technique (VCCT) with uniformly

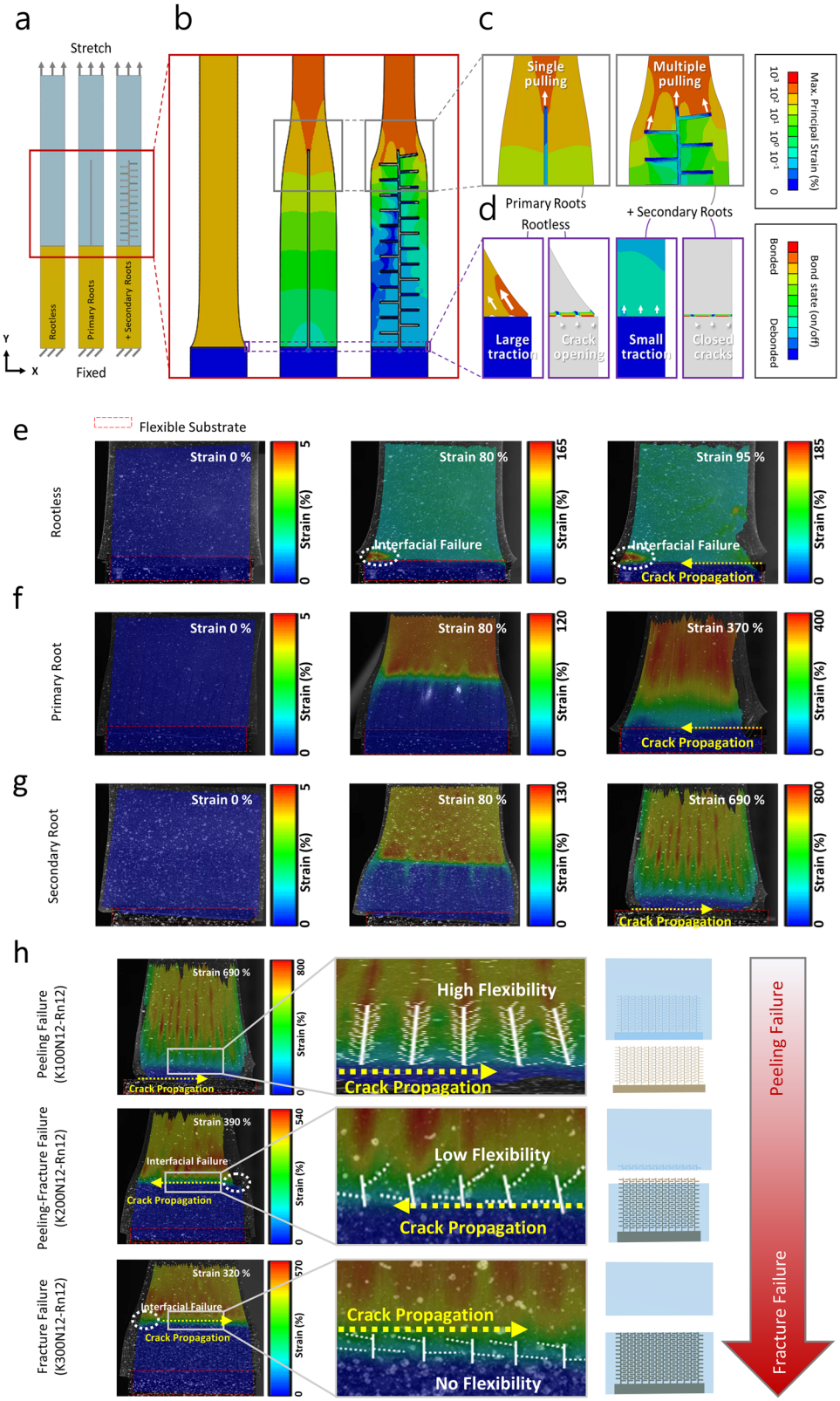


Fig. 4 | Investigation on mechanical behavior of the BIEFI. a Representative models for finite element analysis (FEA). **b** Enlarged strain plot at the 80% strain. **c** Comparison of pulling forces at the tips of root structures. **d** Comparison of traction and crack opening behavior at the right edge of the interface. **e**, **f**, and **h** Digital image correlation (DIC) image demonstrating interfacial failure and crack propagation in (**e**) rootless, (**f**) primary roots, and (**g**) secondary roots. **h** Digital image correlation (DIC) images show evolution from the peeling failure for K100N12-Rn12 to the fracture failure for K300N12-Rn12. The root structures are highlighted in white dotted lines.

distributed microcracks. The detailed information is presented in Supplementary Fig. 11 and the experimental section.

Figure 4b illustrates the stress distribution effect of the primary root by plotting the maximum principal strain at the externally applied strain of 80%. Since the extension in the *y*-direction by external stretch is suppressed due to the bonding with the primary root, it is confirmed that a gradual strain transition between the strain-isolated PI region and the highly strained Ecoflex region can be accomplished with root structures. Moreover, it is also observed that the contraction in the *x*-direction by the Poisson effect shifts from the area near the interface to the area near the end of the primary root. Furthermore, the benefits of secondary roots are presented in Fig. 4c. For the interface only with a primary root, a single pulling force is concentrated at the tip of the primary root, and an interfacial crack simply propagates from the tip of the primary root. On the other hand, for the interface with additional secondary roots, multiple pulling forces exist at each tip of the primary and secondary roots. Especially, pulling forces at each tip of the secondary roots induce the bending of the secondary roots, and their asymmetric features lead to the bending of the primary root. In addition to complicated geometry, the flexible movement of roots deepens the complexity of interfacial crack propagation and results in an enhanced mechanical interlocking effect. Subsequently, as shown in Fig. 4d, small traction is applied at the end of the interface with root structures, and microcracks at the end of the interface are not opened. However, large traction is applied at the rootless interface, and crack opening occurs at the end of the interface, which leads to irreversible interfacial failure from unstable crack propagation. To sum up, the stress distribution effect from the primary roots and the flexible mechanical interlocking effect from the additional secondary roots endow high stretchability to the flexible-to-stretchable platform with BIEFI.

The strain distribution was measured and analyzed during the tensile test to evaluate the effect of roots on the stretchability within BIEFI. In the rootless structure, the interfacial failure between PI island and Ecoflex-0030 occurred at low strain (80% strain) due to poor adhesion between PI and Ecoflex-0030. The crack propagated along the interface at a strain lower than 100% (~95% strain) due to stress concentration at the interfacial failure region (Fig. 4e). The stretchability of the flexible-to-stretchable platform is effectively enhanced by the integration of optimized BIEFI design. The primary roots cause an increase in the adhesion area between PI and Ecoflex-0030, which results in the stress distribution. This phenomenon contributes to increased stretchability, with the primary root exhibiting an enhancement of up to 370% strain (Fig. 4f and Supplementary Fig. 12). Likewise, the secondary root significantly increases the strain energy-consuming area of Ecoflex-0030 by flexible mechanical interlocking effect. The change of strain gradation during the tensile test shows that the stretched Ecoflex-0030 region for secondary root BIEFI slowly progressed toward the PI island. This implies that the flexible mechanical interlocking effect hinders the progression of interfacial failure more effectively in the secondary root compared to the primary root (Supplementary Fig. 13). The exceptional flexibility demonstrated by the secondary root enables it to bend as the roots undergo stretching. Supplementary Figs. 14–16 demonstrates the exceptional flexibility and deformation process of the secondary root under strain. As a result, the stretchability of BIEFI with a secondary root is significantly improved, reaching up to 690% strain without experiencing cracking along the boundary between the secondary root and Ecoflex-0030 (Fig. 4g).

The width of the root plays a critical role in determining the failure mechanism, transitioning from peeling to fracture failure, as depicted in Fig. 4h. The root structures are highlighted with white dotted lines to illustrate their deformation and flexibility under strain prior to failure. When the root width is 100 μm, the structure experiences peeling failure due to the high flexibility provided by the mechanical interlocking effect. As shown by the white dotted lines, the root structure remains highly flexible under applied strain at this width. However, increasing the root width results in greater bending stiffness, reducing its overall flexibility. At a width of 300 μm, the increased stiffness enhances the mechanical interlocking effect, concentrating strain energy at the interface between the root and the Ecoflex-0030 substrate. This concentration of strain energy leads to fracture failure at the interface.

The root structure at 100 μm demonstrates high flexibility, leading to peeling failure, whereas the 300 μm root structure shows minimal flexibility and shifts toward fracture failure. In contrast, at an intermediate width of 200 μm, the root structure exhibits a reduced but still present mechanical interlocking effect, resulting in initial peeling failure followed by fracture failure. As highlighted by the white dotted lines, the 200 μm root retains more flexibility than the 300 μm root but less than the 100 μm root. Therefore, as the root width increases, there is a clear progression from peeling failure to fracture failure, correlating with the reduction in root flexibility (Supplementary Fig. 17).

Mechanical reliability of the BIEFI

The optimized BIEFI design contains two key factors: primary and secondary roots. Primary roots effectively distribute the stress over the BIEFI. On the other hand, secondary roots delay interfacial failure with the flexible mechanical interlocking effect. These factors affect stress distribution and delay interfacial failure, significantly improving stretchability and impacting extreme fatigue life. The two-sided BIEFI specimens are prepared for fatigue tests (Supplementary Fig. 18). Fatigue tests were carried out on RLI at 60% strain and on BIEFI at 130% strain. The interfacial failure could be confirmed by a drop in the strain-stress curve on the *y*-axis[29]. After 69 cycles, accelerated interfacial failure could be observed on the RLI with the drop on the graph (Fig. 5a). On the contrary, BIEFI exhibits significantly robust interfacial behavior for 1000 cycles under higher strain (Fig. 5b). To assess failure under poking deformation at 60% strain, cyclic pressure of 1.75 kPa (compressive force: 0.3 N, depth: 18 mm) was applied to the RLI and BIEFI that were embedded into Ecoflex (Fig. 5c). Figure 5d illustrates the variation in pressure (P/P_0) with respect to the number of applied poking cycles. In case of RLI, interfacial failure arises at the 10th cycle of poking. Failure of the RLI structure is shown in the inset image in Fig. 5d. On contrary, the BIEFI remained reliable interface for the duration of 1000 cycles (Fig. 5d). This outcome indicates that the BIEFI effectively inhibits failure through applied shear stress by poking. To validate the mechanical integrity of omnidirectional BIEFI when subjected to twisting, we applied a cyclic tensile strain of 60% to RLI and BIEFI at twisting angles of 180° and 360° (Fig. 5e and Supplementary Fig. 19). In Fig. 5f, the graph illustrates the relative change in the modulus over the cycles. When cyclically stretched at a twisting angle of 180° for RLI, the E/E_0 ratio decreased under 0.95, corresponding to interfacial failure, around 20 cycles. After 50 cycles, the E/E_0 ratio decreased under 0.85, corresponding to failure of the RLI. Conversely, the E/E_0 ratio of the BIEFI maintained a relatively stable value of 0.98 when twisted at 180° and 0.99 when twisted at 360°, suggesting a highly stable structure under torsional stress.

Applications of BIEFI to diverse stretchable electronics

Various approaches have been explored to connect stretchable electronics and to demonstrate their potential in diverse areas. The serpentine structure is commonly used to link one flexible island to another. Since excessive stretching can cause irreversible deformation in the serpentine structures, an elongation range of only 20% to 50% can be accommodated. Thus, the serpentine structure is not ideal for highly stretchable electronics. Since previous research has shown Ag flake/Ecoflex-0030-based intrinsically stretchable electrodes perform well under excessive stretching, these stretchable electrodes are used

https://doi.org/10.1038/s41467-025-56502-9

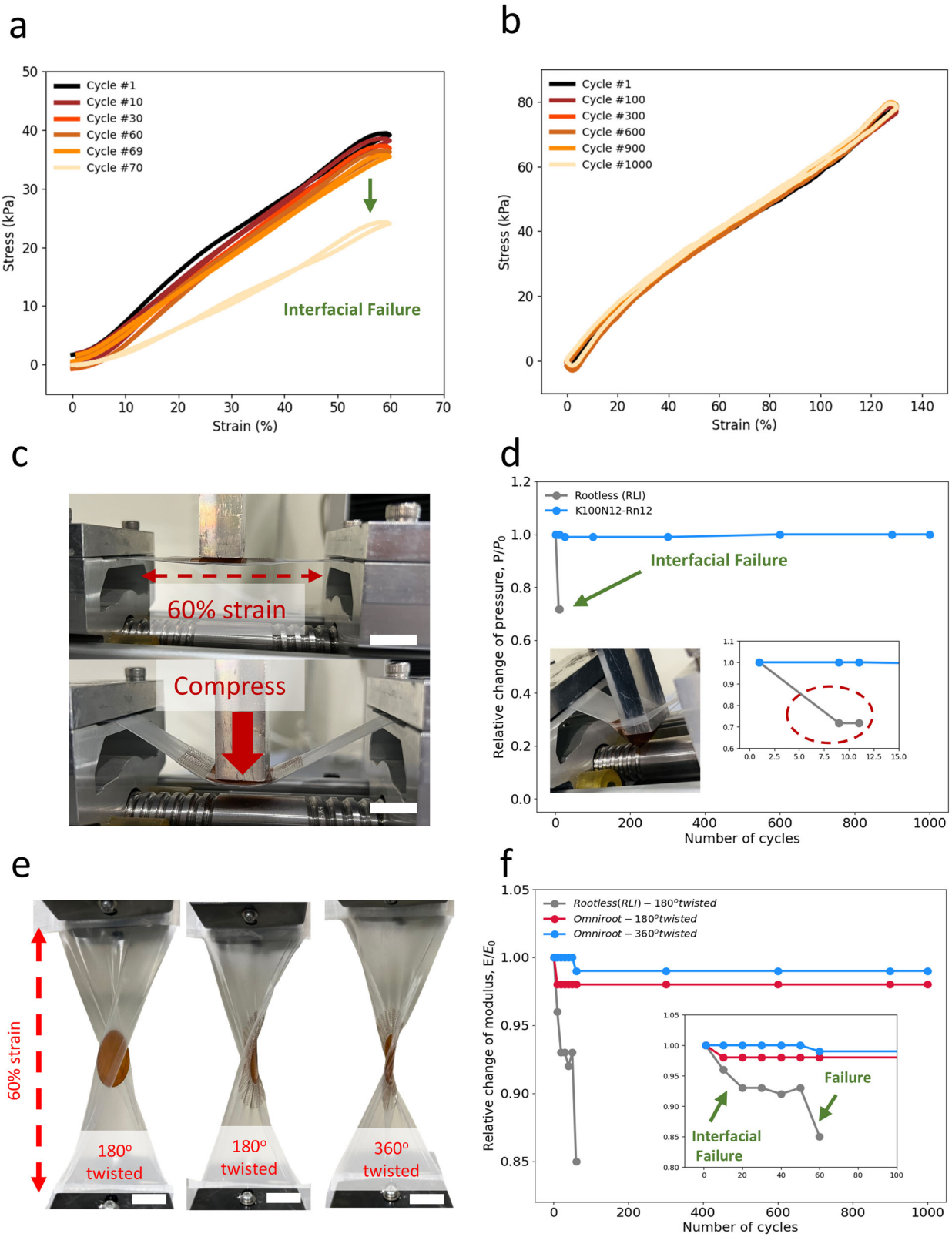


Fig. 5 | Flexible-to-stretchable platform under diverse physical deformations. **a**, **b** Stress versus strain graph of (**a**) RLI (**b**) BIEFI under cyclic strain of 60% and 130% (**c**) Photographs of BIEFI with 60% strain under cyclic pressure of 1.75 kPa (force: 0.3 N). Scale bar = 15 mm. **d** Relative change of pressure (P/P_0) versus cycle for RLI and BIEFI under cyclic poking. The inset on the right provides a zoom-in of the curve at 0 to 15 cycles. The inset on the left demonstrates the failure of RLI after 10 cycles. **e** Photographs of twisted omnidirectional RLI (180°) and BIEFI (180° and 360°) for cyclic strain of 60%. Scale bar 20 mm. **f** Relative change of modulus (E/E_0) versus cycles for twisted strain experiment of omnidirectional RLI and BIEFI. The inset demonstrates a zoom-in of the curve at 0 to 100 cycles. Source data are provided as a Source Data file.

https://doi.org/10.1038/s41467-025-56502-9

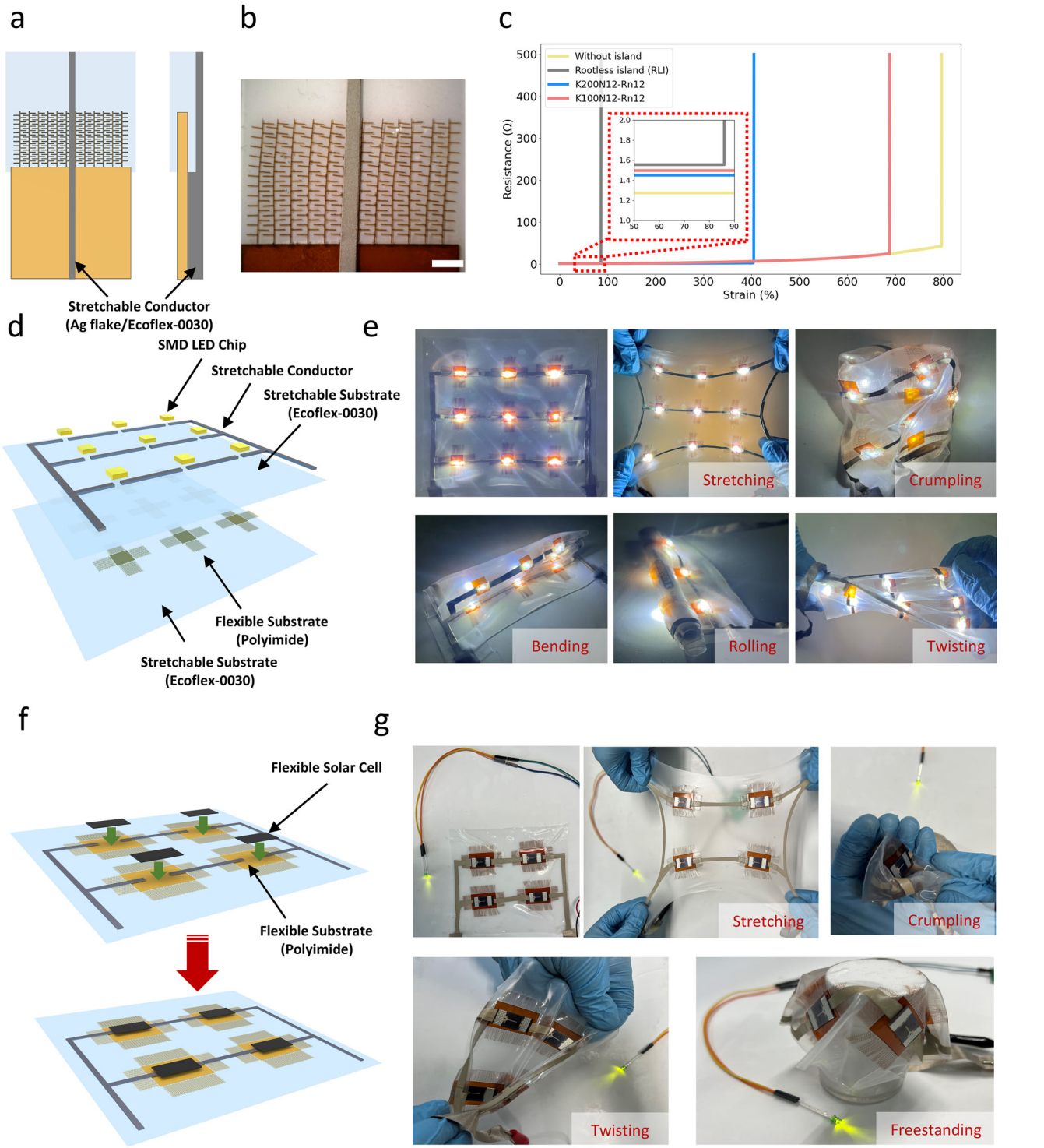


Fig. 6 | Stretchable electronics applications of BIEFI with diverse electronic devices. a Schematic illustration of the intrinsically stretchable electrode on the BIEFI platform. **b** Photograph of the printed intrinsically stretchable electrode on the BIEFI platform. Scale bar = 3 mm. **c** Resistance versus strain for the printed intrinsically stretchable electrode on different design cases. The inset demonstrates a zoom-in of the curve at 50% to 90% strain. **d** Schematic illustration of stretchable LED array. **e** Photograph of the stretchable LED array under diverse physical deformations (stretching, crumpling, bending, rolling, and twisting) (**f**) Schematic illustration of the stretchable array of flexible solar cells. **g** Photograph of the stretchable array of flexible solar cells under various physical deformations (stretching, crumpling, twisting, and freestanding). Source data are provided as a Source Data file.

to connect one island to another. (Fig. 6a, b and Methods)[30]. The intrinsically stretchable electrode was screen-printed using a polyethylene terephthalate (PET) mask. Figure 6c demonstrates the strain at failure for various design cases with screen-printed stretchable electrodes. While the RLI shows electrical failure around 100% strain, the K200N12-Rn12 and K100N12-Rn12 design cases demonstrate electrical failure around 400% and 700% strain, respectively. Furthermore, a photodetector experiment was conducted to evaluate the stability and performance of the stretchable conductor integrated with an LED under strain. While the RLI exhibited failure at approximately 90%

strain, the BIEFI not only maintained stable conductivity but also supported the stable operation of the LED even at strains exceeding 650% (Supplementary Figs. S20 and S21). These results demonstrate that the BIEFI system effectively preserves both electrical performance and device functionality under extreme mechanical deformation, highlighting its suitability for highly stretchable functional device applications. These results indicate that the stretchable electrode does not prevent interfacial failure; when interfacial failure occurs, the electrical connection is immediately disrupted. The intrinsically stretchable electrode without island shows electrical failure at 800% strain as a result of elastomer failure. According to the obtained results, the intrinsically stretchable electrode is suitable for a wide range of applications in highly stretchable electronics.

The BIEFI design was positioned around the island to fabricate biaxially stretchable electronics. The islands were prepared to create a 3 × 3 stretchable LED array (Fig. 6d and Methods). After the embedment of the islands, stretchable electrodes were printed using the stencil printing method with a prepared mask. SMD LED chips were mounted on each island and securely fixed with Sil-Poxy. The fabricated stretchable LED array effectively performs operations under various physical deformation types, such as stretching, crumpling, bending, rolling, and twisting (Fig. 6e and Supplementary Movie 1). The stretchable LED array exhibits reliable performance across various deformation modes, suggesting a promising outlook for stretchable displays. Furthermore, a 2 × 2 array of flexible solar cells was placed on islands for energy harvesting to save energy for a battery, subsequently powering an LED (Fig. 6f). The fabricated stretchable solar cell powered the LED under diverse physical deformation types such as stretching, crumpling, twisting, and freestanding (Fig. 6g). The demonstrated stretchable LED and solar cell arrays highlight how the proposed flexible-to-stretchable platform with BIEFI can safely function in diverse situations with a variety of electronic products. This highly stretchable, flexible-to-stretchable platform can play a pivotal role in integrating energy harvesting, storage, and device-powering structures, thereby laying the foundation for comprehensive stretchable electronics in future wearable device applications.

The proposed BIEFI structure exhibits excellent stretchability and enduring performance under repeated physical deformations for the flexible-to-stretchable platform. A resistance band experiences repeated extreme physical deformations with high stretchability. Hence, it becomes imperative to establish a device that ensures signal integrity amidst diverse physical deformations. To exemplify the practicality of the BIEFI structure, we fabricated a smart resistance band that demands an exceptionally highly stretchable and durable framework for enduring repeated physical deformations. Figure 7a shows the multi-layered device structure of the smart resistance band, including a pair of Arduino Nano 33 BLE, flexible islands (BIEFI), a strain sensor, stretchable electrodes, and stretchable substrates. The smart resistance band consists of two accelerometers and a carbon nanotube (CNT) based strain sensor[31], which is a CNT layer coated on the Ecoflex. The Arduino Nano 33 BLE, which consists of an accelerometer, was placed on each BIEFI to monitor acceleration, while the CNT-based sensor was strategically placed between the two BIEFI structures to monitor strain (Fig. 7b). The device fabrication and assembly details of the smart resistance band appear in Methods section. The real-time recorded movie clip in Supplementary Movie 2 demonstrates the efficacy of the BIEFI-based smart resistance band from the applied strain and movements. The strain and accelerometer data collected were transmitted to the computer by the Bluetooth module integrated with the Arduino Nano 33 BLE (Supplementary Fig. 22). Workout monitoring was conducted using the smart resistance band for exercises such as back fly, standing leg abductions, and side-lying hip abduction. For exercises, achieving a balanced workout is essential to ensure simultaneous engagement of both sides of the muscles. Hence, back fly exercise is monitored for right-handed, left-handed, and balanced workouts, as depicted in Fig. 7c. Furthermore, standing leg abductions and side-lying hip abduction exercises are monitored for both fast and slow-motion variations (Fig. 7d, e). The accelerometer data provides a detailed analysis of dynamic movements during exercises, measuring acceleration along multiple axes to reflect both the direction and speed of motion. Simultaneously, the strain data quantifies the extent to which the resistance band is stretched during exercise, illustrating variations in tension corresponding to different motion intensities. The integration of accelerometer and strain data provides a thorough understanding of the user's interaction with the resistance band, enabling detailed feedback for the analysis of exercise performance.

For practical applications, the development of stretchable healthcare devices is crucial to support diverse functionalities. Pulse rate and pulse waveforms serve as vital physiological indicators for quantitatively assessing cardiovascular health and overall well-being. Their noninvasive and continuous monitoring is essential for diagnostic and prognostic purposes in various healthcare applications. The versatile BIEFI platform facilitates the seamless integration of multiple sensors while preserving stretchability. Accordingly, a photoplethysmography (PPG)-based pulse sensor was integrated into the BIEFI platform to evaluate its potential as a healthcare monitoring device (Fig. 7f and Methods). The fabricated stretchable wrist-type pulse sensor module was affixed to a human forearm to capture pulse signals from the PPG sensor. Figure 7g displays the pulse waveform acquired by the module, revealing a measured pulse rate of 69 beats per minute. Furthermore, Fig. 7h illustrates a single-region measurement of the pulse pattern, highlighting systolic and diastolic phases along with the dicrotic notch. These findings highlight the transformative potential of the BIEFI platform in advancing next-generation stretchable and wearable healthcare technologies, paving the way for seamless, real-time cardiovascular monitoring and personalized health management systems.

Discussion

In this study, we proposed a BIEFI design for a flexible-to-stretchable platform to achieve high stretchability and superior usage life. We systematically investigated the effect of parameters on roots-soil-inspired design, such as primary roots, secondary roots, and width of the roots. Notably, the effect of stress distribution (primary roots) and flexible mechanical interlocking (secondary roots) delay and suppress the interfacial failure in the flexible-to-stretchable substrate interface. Importantly, the optimized BIEFI design realizes superior extended fatigue life under diverse physical deformations. LEDs and solar cells were utilized to demonstrate the diverse applicability of the BIEFI on flexible-to-stretchable electronics. Furthermore, a smart resistance band was developed to quantify workouts by integrating electronics into the BIEFI within the resistance band. Our research provides a promising strategy for developing and commercializing stretchable electronics in the coming years.

Despite the accomplishments mentioned earlier, there are still opportunities to enhance the proposed flexible-to-stretchable platform through various approaches. First, a unidirectional parameter study is conducted and demonstrated in the applications, exhibiting the feasibility of omnidirectional design. This suggests an opportunity to design an omnidirectional interface with relevant parameter studies. The omnidirectional interface design will expand more potential application opportunities to the flexible-to-stretchable platform. Second, in this study, the effect of the adhesion parameter on stretchability was not explored. Nevertheless, the adhesion force between PI and Ecoflex substrate can be investigated through various methodologies. The increased adhesion of PI to elastomer will enhance the gripping effect of the roots, leading to improved strain at failure value. Third, the proposed root designs are relatively simplistic, consisting of only a straight configuration of primary and secondary roots. In reality,

https://doi.org/10.1038/s41467-025-56502-9

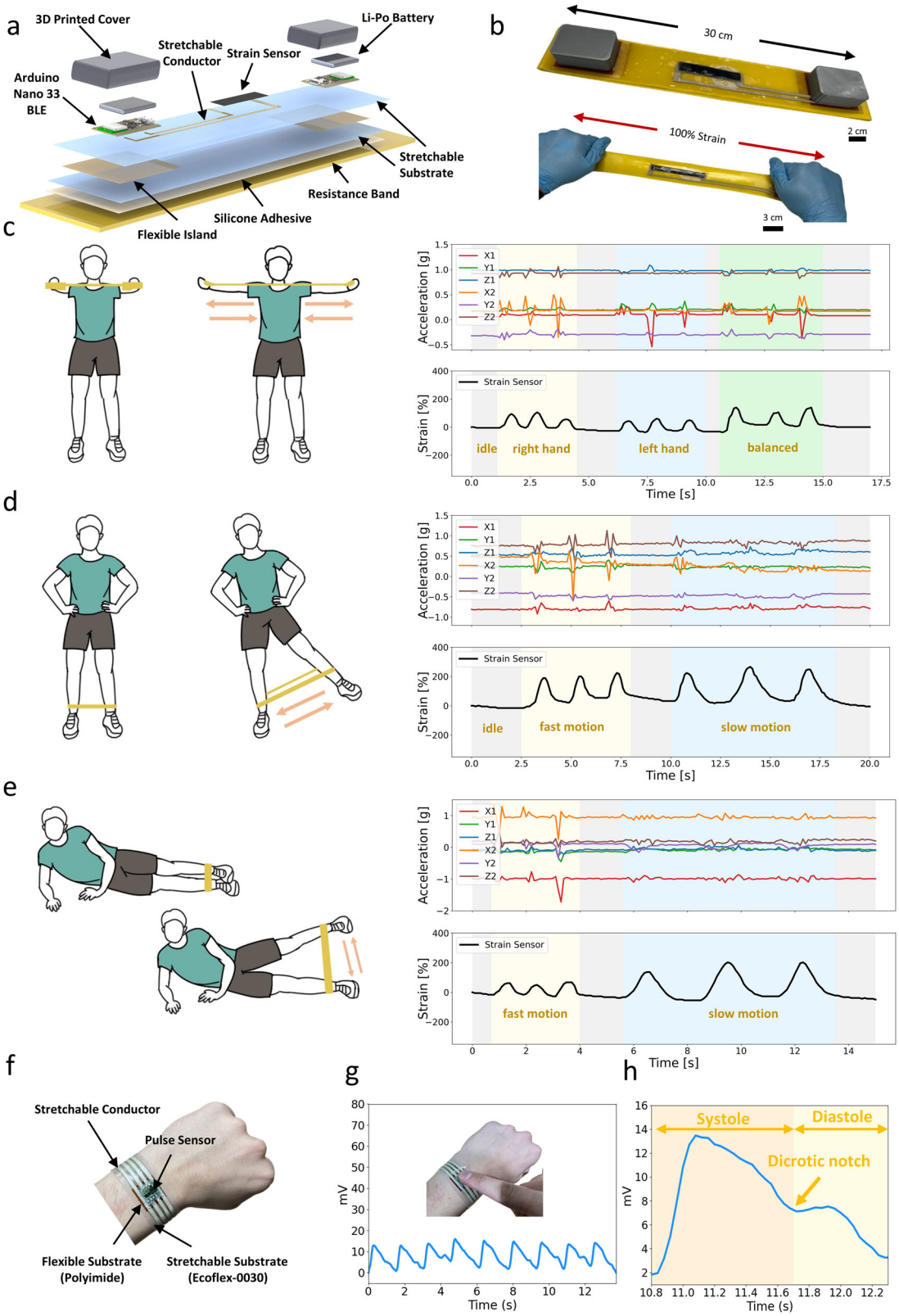


Fig. 7 | Wearable healthcare monitoring with sensors on a BIEFI platform. **a** Schematic illustration of smart resistance band. **b** Photograph of the smart resistance band with/without applied strain. **c** Left: Schematic illustration of the back fly with the smart resistance band. Right: Workout data (acceleration and strain) for the back fly workout. Right-handed, left-handed, and balanced back fly workout. **d**, **e** Left: Schematic illustration of (**d**) standing leg abductions (**e**) side-lying hip abduction workout with the resistance band. Right: Workout data for (**d**) standing leg abductions (**e**) side-lying hip abduction with fast and slow motions. **f** Photograph of stretchable wrist type pulse sensor on BIEFI platform. **g** Graph of PPG pulse wave detected by the stretchable wrist type pulse sensor. The inset image demonstrates pulse measurement. **h** Single-region pulse wave measurement. Source data are provided as a Source Data file.

plant roots show a high degree of complexity, which allows them to have a strong gripping effect on the soil. Mimicking this complex design could also provide a higher degree of strain at failure value and stability performance for the flexible-to-stretchable platform.

The developed highly stretchable and durable flexible-to-stretchable platform with BIEFI provides a promising strategy for integrating rigid, flexible, and stretchable components; thereby, the platform can be used in many various applications, such as stretchable displays, energy storage devices, medical devices, and so on. Our strategy promises a future in which the flexible-to-stretchable platform effortlessly elevates and redefines the electronics world.

Methods

Fabrication of flexible island for tensile test

The BIEFI specimens were fabricated using the UV laser-cutting method. The root designs were created using a 3D computer-aided design (CAD) program (Fusion 360, Autodesk, USA). After modeling the roots, the 3D CAD file was converted to a DXF file, which was then imported into the UV laser-cutting software (KEYENCE Marking Builder, Japan). Polyimide (PI) film (SKC KOLON PI, Korea) was prepared and placed in the UV laser-cutting machine (MD-U1000C, KEYENCE, Japan). The UV laser cutting conditions include a laser power set at 80%, a scan speed of 300 mm/s, a pulse frequency of 40 kHz, and a printing number of 20. After the laser-cutting operation, the final patterned PI was peeled from the PI film.

A releasing agent (ER-200, Smooth-On Inc., USA) was coated on the soda-lime glass (Nippon Sheet Glass, Japan) to release the stretchable substrate. Ecoflex-0030 was prepared by mixing its components, A and B, with a ratio of 1:1 with a planetary mixer (Thinky ARM-310, USA) to perform a mixing time of 2 min at 2000 rpm and a deformation time of 10 s at 2200 rpm. The soda-lime glass was spin-coated (900 rpm, 20 s) with prepared Ecoflex-0030 and cured at 80 °C for 30 min. Then, the prepared patterned PI was placed onto the Ecoflex-0030. Additional Ecoflex-0030 mixture was prepared and spin-coated (500 rpm, 20 s) to encapsulate the patterned PI. The obtained specimen was cured at 80 °C for 30 min. After the curing process, the specimen was prepared by cutting into a size of 50 × 22 mm. Finally, the specimen was cut for the tensile test to recognize interfacial failure between flexible and stretchable substrates.

Tensile-related tests

For all tensile tests, a universal testing machine (AG-X plus, Shimadzu, Japan) and a load cell (SBL-1KN, Shimadzu, Japan) capable of measuring up to 1kN force is used to measure the applied force. Pneumatic flat grips (Shimadzu, Japan) were used to securely grasp the specimens for each experiment. The speed was set to 50 mm/min for each test.

To measure the strain at failure of omnidirectional design (Fig. 3i), the specimen is applied to vertical directional strain. In each test, the position of the specimen is rotated at a 60° angle.

FEA simulation

Mechanical behavior of rootless interface, interface with a primary root, and that with additional secondary roots were simulated using a commercial finite element analysis software (Abaqus v 6.24, Dassault Systemes, France). Each model consisted of a deformable 2D solid with ~530,000 elements of type CPS4R (4-node bilinear plane stress quadrilateral, reduced integration, hourglass control). The flexible PI root structures were considered to be purely elastic, while the stretchable Ecoflex grounds were considered to be hyperelastic based on the Ogden model. The elements at the interface were bonded with VCCT, and the interfacial fracture energy (Gc) was assumed to be 10 J/m^2, considering moderate energy dissipation in hyperelastic material. In addition, microcracks with length of ~20 μm were uniformly distributed at the interface to simulate the small-scale crack opening and subsequent crack propagation. To effectively adopt two coupled criteria for interfacial debonding between dissimilar materials[24,32], microcracks were placed at the points including the critical points of maximum normal traction for simulating the crack onset, while interfacial crack propagation was simulated by incrementally comparing the energy release rate (G) and the assumed value of Gc in the direction of maximum tangential stress. After further experimental investigation, the assumed value of Gc is found to be plausible as discussed in Supplementary Fig. 23 and accompanying Supplementary Note.

Digital image correlation for strain mapping

Strain distribution on the surface of the BIEFI specimens was calculated and analyzed using a commercial DIC algorithm program (ARAMIS, Gesellschaft für Optische Messtechnik mbH) with 0.005% error for strain measurement. For strain measurements, white speckle patterns were randomly generated on the surface of the BIEFI specimens by commercial ceramic spray (SF 7900, LOCTITE, Germany), and two charge-coupled device (CCD) cameras (6 million pixels) were calibrated to measure the proper area (30 × 24 mm). Analyzed images were captured at 3 Hz by the two CCD cameras during the tensile test at a strain rate of 50 mm/min using a universal testing machine (AGS-X, SHIMADZU, Japan). The equivalent Mises strain distribution within the boundary region between the PI root and Ecoflex-0030 was analyzed by applying the interpolation method that calculates the strain in the boundary region as the average value of the strains of the PI root and Ecoflex-0030.

Fabrication of intrinsically stretchable electrode

The intrinsically stretchable electrode used in this study was based on an Ag Flake/ Ecoflex, as described in a previous study[30]. MIBK (4-methyl-2-pentanone) (Daejung Chemical & Metals, Korea) and Ecoflex-0030 were mixed in a 3:3 ratio with a planetary mixer (mixing time of 2 min and a deformation time of 10 s). Ag flakes (Daejoo Electronic Materials, Korea) added into the obtained mixed solution as the ratio of 14, then mixed again with the planetary mixer at the same conditions above. Subsequently, the obtained final solution of Ag flake/Ecoflex/MIBK was stencil printed on the prepared islands through a Polyethylene (PE) mask of thickness of 200 μm.

The MIBK solvent was subjected to evaporation at 80 °C for 1 h. The Ag flake/Ecolex solution was thermally sintered at 110 °C for 2 h to accomplish electrical conductivity of 4006 S cm^{-1}).

Electrical stability test of intrinsically stretchable electrode

To measure the electrical stability of intrinsically stretchable electrodes with integration to the developed flexible-to-stretchable platform, woven conductive fabric (Shzhou Wanhe Electronic, China) was utilized to connect the intrinsically stretchable electrodes to Arduino Due. The resistance of the intrinsically stretchable electrode was measured using a reference resistor in series to create a voltage-dividing circuit.

Fabrication of stretchable LED array and stretchable solar cell array

Ecoflex-0030 was spin-coated onto a soda-lime glass (150 × 150 mm). To install a surface mount device (SMD) LED chip, the dimensions of the island were adjusted to 10 × 10 mm (root length: 10 mm), the array was prepared as 3 × 3 on the Ecoflex substrate, and the center-to-center distance of 40 mm was designed between the islands. Then, Ecoflex-0030 was spin-coated onto the islands for embedment. Ag flake/Ecoflex/MIBK solution was stencil printed on the islands with the PE mask. After the curing of the intrinsically stretchable electrode, SMD LED chips (HSUKWANG, China) were mounted on each island. As the SMD LED chips show insecure placement, they are fixed with Silpoxy (Smooth-On Inc., USA). Woven conductive fabric (Shzhou Wanhe Electronic, China) was utilized to connect intrinsically stretchable

electrode to electric wires. A bias of 12 V was applied to turn on the SMD LED chips. As the flexible solar cell had a dimension of 23 × 12 mm, the dimension of BIEFI was adjusted to 20 × 30 mm with a root length of 10 mm. After embedding the islands into the Ecoflex-0030, stencil printing and curing process of the Ag flake/Ecoflex/MIBK were conducted. The flexible solar cells were mounted onto each island and fixed at the edge area with Silpoxy. A fabricated stretchable solar cell array was connected to a DEV-BASIC (PowerFilm Inc.) module to store the solar energy in a battery and to power the LED.

Fabrication of smart resistance band

For the fabrication of smart resistance band, two BIEFI (50 × 40 mm) samples were embedded in Ecoflex (45 × 300 mm). The fabrication process and screen printing of the stretchable electrodes on the Ecoflex are the same as in previous applications. The preparation of CNT-based strain sensor was conducted in accordance with the previously reported work. The two BIEFI structures were mounted on two opposite sides of the Ecoflex layer, with the strain sensor positioned in the middle. Two Arduino Nano 33 BLE boards were placed onto the two BIEFI structures. Rechargeable lithium-ion batteries powered the Arduino boards (3.7 V, 80 mAh). The final product was adhered with Sil-Poxy to the commercial resistance band (light resistance band, Up & Shape, China). The strain sensor was connected to the 3.3 V supply and an analog pin on the Arduino for the purpose of reading resistance values. The covers were fabricated using a 3D printer (Ultimaker 3S, USA) to package the measurement system of the smart resistance band. The BLE modules of the Arduino were utilized to transmit the data of the measured resistance and acceleration to the computer (Supplementary Fig. 12). These experiments were conducted with the approval of the Institutional Review Board (IRB) at the Korea Advanced Institute of Science and Technology (KAIST) under protocol number KH2024-200, and informed consent was also obtained from the volunteer (one of the authors of this paper) for wearable testing.

Fabrication of stretchable pulse sensor module

To fabricate the stretchable pulse sensor module, the MAX30101 optical sensor (Maxim Integrated Products, Inc.) was employed. Initially, Ecoflex-0030 was spin-coated onto a 100 × 100 mm soda-lime glass substrate to form a flexible base layer. The BIEFI platform was subsequently positioned on the Ecoflex-0030 layer, followed by an additional spin-coating process to encapsulate it. A stretchable electrode was then screen-printed onto the BIEFI platform. Finally, the MAX30101 sensor was securely affixed using Silpoxy, and electrical connections were established through the stretchable electrode.

Reporting summary

Further information on research design is available in the Nature Portfolio Reporting Summary linked to this article.

Data availability

All data supporting the findings of this study are available within the article and its supplementary files. Any additional requests for information can be directed to, and will be fulfilled by, the corresponding authors. Source data are provided with this paper.

References

1. Kim, D. W., Kong, M. & Jeong, U. Interface design for stretchable electronic devices. *Adv. Sci.* **8**, 2004170 (2021).
2. Kim, M. S. et al. Skin-like omnidirectional stretchable platform with negative poisson's ratio for wearable strain–pressure simultaneous sensor. *Adv. Funct. Mater.* **33**, 2208792 (2023).
3. Kim, M. S. et al. Stretchable printed circuit board based on leak-free liquid metal interconnection and local strain control. *ACS Appl. Mater. Interfaces* **14**, 1826–1837 (2021).
4. Choi, J. et al. Customizable, conformal, and stretchable 3D electronics via predistorted pattern generation and thermoforming. *Sci. Adv.* **7**, eabj0694 (2021).
5. Cho, S. et al. Wireless, multimodal sensors for continuous measurement of pressure, temperature, and hydration of patients in wheelchair. *npj Flex. Electron.* **7**, 8 (2023).
6. Oh, Y. S. et al. Battery-free, wireless soft sensors for continuous multi-site measurements of pressure and temperature from patients at risk for pressure injuries. *Nat. Commun.* **12**, 5008 (2021).
7. Rogers, J. A., Someya, T. & Huang, Y. Materials and mechanics for stretchable electronics. *Science* **327**, 1603–1607 (2010).
8. Jeong, Y. et al. Ultra-wide range pressure sensor based on a microstructured conductive nanocomposite for wearable workout monitoring. *Adv. Healthc. Mater.* **10**, 2001461 (2021).
9. Gul, O. et al. Sensitivity-controllable liquid-metal-based pressure sensor for wearable applications. *ACS Appl. Electron. Mater.* **3**, 4027–4036 (2021).
10. Choi, J. et al. Wearable self-powered pressure sensor by integration of piezo-transmittance microporous elastomer with organic solar cell. *Nano Energy* **74**, 104749 (2020).
11. Kim, N. et al. Stretchable inorganic LED displays with double-layer modular design for high fill factor. *ACS Appl. Mater. Interfaces* **14**, 4344–4351 (2022).
12. Biswas, S. et al. Integrated multilayer stretchable printed circuit boards paving the way for deformable active matrix. *Nat. Commun.* **10**, 4909 (2019).
13. Vallem, V. et al. Energy harvesting and storage with soft and stretchable materials. *Adv. Mater.* **33**, 2004832 (2021).
14. Jung, Y. et al. Spherical micro/nano hierarchical structures for energy and water harvesting devices. *Small Methods* **6**, 2200248 (2022).
15. Lee, J.-W. et al. Rigid-and soft-block-copolymerized conjugated polymers enable high-performance intrinsically stretchable organic solar cells. *Joule* **8**, 204–223 (2024).
16. Xue, Z. et al. Mechanically-guided structural designs in stretchable inorganic electronics. *Adv. Mater.* **32**, 1902254 (2020).
17. Hou, S. et al. Stretchable electronics with strain-resistive performance. *Small* **20**, 2306749 (2024).
18. Kim, R.-H. et al. Waterproof AlInGaP optoelectronics on stretchable substrates with applications in biomedicine and robotics. *Nat. Mater.* **9**, 929–937 (2010).
19. Haque, A. T., Hwang, D. & Bartlett, M. D. Graded kirigami composites for programmed strain distributions. *Adv. Mater. Technol.* **7**, 2101241 (2022).
20. Libanori, R. et al. Stretchable heterogeneous composites with extreme mechanical gradients. *Nat. Commun.* **3**, 1265 (2012).
21. Oh, E. et al. Modulus-gradient conductive core–shell structures formed by magnetic self-assembling and printing processes for highly stretchable via applications. *Adv. Electron. Mater.* **3**, 1600517 (2017).
22. Matsuhisa, N. et al. Printable elastic conductors with a high conductivity for electronic textile applications. *Nat. Commun.* **6**, 7461 (2015).
23. Naserifar, N., LeDuc, P. R. & Fedder, G. K. Material gradients in stretchable substrates toward integrated electronic functionality. *Adv. Mater.* **28**, 3584–3591 (2016).
24. Yang, J. C. et al. Geometrically engineered rigid island array for stretchable electronics capable of withstanding various deformation modes. *Sci. Adv.* **8**, eabn3863 (2022).
25. Zhu, M., Zhang, F. & Chen, X. Bioinspired mechanically interlocking structures. *Small Struct.* **1**, 2000045 (2020).
26. Liu, Z. et al. High-adhesion stretchable electrodes based on nanopile interlocking. *Adv. Mater.* **29**, 1603382 (2017).

27. Jin, T. et al. Bioinspired, tree-root-like interfacial designs for structural batteries with enhanced mechanical properties. *Adv. Energy Mater.* **11**, 2100997 (2021).
28. Wallin, T. J. et al. 3D printable tough silicone double networks. *Nat. Commun.* **11**, 4000 (2020).
29. Liao, Z. et al. A comprehensive thermo-viscoelastic experimental investigation of Ecoflex polymer. *Polym. Test.* **86**, 106478 (2020).
30. Kim, S. H. et al. Ultrastretchable conductor fabricated on skin-like hydrogel–elastomer hybrid substrates for skin electronics. *Adv. Mater.* **30**, 1800109 (2018).
31. Amjadi, M., Yoon, Y. J. & Park, I. Ultra-stretchable and skin-mountable strain sensors using carbon nanotubes–Ecoflex nanocomposites. *Nanotechnology* **26**, 375501 (2015).
32. Mantič, V. Interface crack onset at a circular cylindrical inclusion under a remote transverse tension. Application of a coupled stress and energy criterion. *Int. J. Solids Struct.* **46**, 1287–1304 (2009).

Acknowledgements

I.P. was supported by the National Research Foundation of Korea (NRF) grant funded by the Korean government (MSIT) (No. 2021R1A2C3008742). T-S. K. was supported by the National Research Foundation of Korea (NRF) grant funded by the Korea government (MSIT) (No. 2022R1A2C3009087). H.J.K. was supported by the Institute of Information & communications Technology Planning & Evaluation (IITP) grant funded by the Korean government (MSIT) (No. 2022-0-00025, Development of soft-suit technology to support human motor ability).

Author contributions

O.G. and I.P. led the development of the concepts, designed the experiments, and interpreted the results; M.S. carried out the simulation of design; C.Y.G. conducted the experiment on DIC analysis; O.G. led the experimental work with support from Jihyeon A., K.L., Junseong A.; H.J.K, T-S. K., I.P. directed the project.

Competing interests

The authors declare no competing interests.

Additional information

Supplementary information The online version contains supplementary material available at https://doi.org/10.1038/s41467-025-56502-9.

Correspondence and requests for materials should be addressed to Hye Jin Kim, Taek-Soo Kim or Inkyu Park.

Peer review information *Nature Communications* thanks Zheng Yan, and the other, anonymous, reviewer(s) for their contribution to the peer review of this work. A peer review file is available.

Reprints and permissions information is available at http://www.nature.com/reprints

Publisher's note Springer Nature remains neutral with regard to jurisdictional claims in published maps and institutional affiliations.

Open Access This article is licensed under a Creative Commons Attribution-NonCommercial-NoDerivatives 4.0 International License, which permits any non-commercial use, sharing, distribution and reproduction in any medium or format, as long as you give appropriate credit to the original author(s) and the source, provide a link to the Creative Commons licence, and indicate if you modified the licensed material. You do not have permission under this licence to share adapted material derived from this article or parts of it. The images or other third party material in this article are included in the article's Creative Commons licence, unless indicated otherwise in a credit line to the material. If material is not included in the article's Creative Commons licence and your intended use is not permitted by statutory regulation or exceeds the permitted use, you will need to obtain permission directly from the copyright holder. To view a copy of this licence, visit http://creativecommons.org/licenses/by-nc-nd/4.0/.

© The Author(s) 2025